IEEE Access
Multidisciplinary ⋮ Rapid Review ⋮ Open Access Journal

Received 14 December 2024, accepted 14 January 2025, date of publication 20 January 2025, date of current version 27 January 2025.

Digital Object Identifier 10.1109/ACCESS.2025.3531979

RESEARCH ARTICLE

A Quantum-Based Machine Learning Approach for Autism Detection Using Common Spatial Patterns of EEG Signals

S. SARANYA[1] **AND R. MENAKA**[2]
[1]School of Electronics Engineering, Vellore Institute of Technology, Chennai, Tamil Nadu 600127, India
[2]Centre for Cyber Physical Systems, Vellore Institute of Technology, Chennai, Tamil Nadu 600127, India

Corresponding author: R. Menaka (menaka.r@vit.ac.in)

This work was supported by Vellore Institute of Technology, Chennai.

This work involved human subjects in its research. Approval of all ethical and experimental procedures and protocols was granted by the Institutional Ethics Committee of Sri Ramachandra Institute of Higher Education and Research under Reference No. IEC/18/OCT/144/41, and performed in line with the Declaration of Helsinki.

ABSTRACT Autism Spectrum Disorder (ASD) significantly impacts social communication, interaction, and behavior. Early diagnosis and timely intervention can improve outcomes by enabling tailored therapeutic strategies. Electroencephalography (EEG) has emerged as a non-invasive tool to capture brain activity and facilitate the early detection of ASD using machine learning techniques. However, attaining high accuracy with minimal EEG channels remains a challenge. This study analyzed EEG data from 10 children with ASD and 10 Typically Developed (TD) children using three electrode combinations: C3-C4, C3-Cz, and C4-Cz. EEG signals were spatially filtered using a wavelet-based regularized filter bank common spatial pattern. Key features, including peak-to-peak amplitude, were extracted, and correlation-based feature selection identified the most informative features. Classification with Support Vector Machine (SVM) identified the C4-Cz pair as the most effective, achieving the highest accuracy. Further analysis applied Neural Networks (NN), Quantum Support Vector Machines (QSVM), and Quantum Neural Networks (QNN) to classify data from the C4-Cz pair. QSVM with amplitude embedding feature map outperformed others, achieving an accuracy of 94.7%. Performance was further improved by incorporating an enhanced feature set comprising peak frequency, Stockwell transform coefficients, and peak-to-peak amplitude. The proposed system, leveraging these refined features and QSVM, achieved an exceptional accuracy of 98.9%. To our knowledge, this is the first study utilizing an enhanced feature set derived from reduced brain lobes and quantum machine learning for ASD classification, offering a novel and highly accurate diagnostic approach.

INDEX TERMS Autism spectrum disorder, quantum neural network, quantum support vector machine, wavelet, common spatial pattern.

I. INTRODUCTION

Autism Spectrum Disorder (ASD) is a complex neurological and developmental disorder. The complicated and poorly understood etiology of ASD includes neurobiology, genetics, and environmental exposures, resulting in a wide range of presenting behaviors and symptoms. Recent estimates suggest that in 2020, approximately 1 in 36 children aged 8 years were affected by ASD, with boys being four times more likely to be diagnosed compared to girls. This prevalence is higher than previous estimates from 2000 to 2018 [1]. Data is utilized from the Medical Expenditure Panel Survey (MEPS) connected to the National Health Interview Survey (NHIS) Sample Child Core questionnaire to determine ASD case status among 45,944 children aged 3 to 17 years. Data revealed that the additional yearly cost per

The associate editor coordinating the review of this manuscript and approving it for publication was Md Kafiul Islam.

child associated with an ASD diagnosis, compared to children without an ASD diagnosis, ranged from $3930 to $5621 (2018 US dollars), underscoring the substantial financial burden on the United States healthcare system [2]. Understanding the unique perspectives of individuals with autism is paramount for providing adequate support in navigating daily challenges. With an increasing emphasis on early detection, interventions can be implemented swiftly, potentially improving the quality of life for those with ASD [3]. However, numerous barriers contribute to delays in diagnosis, including healthcare provider's discomfort in identifying autism, delayed referrals, and parent's challenges in recognizing developmental concerns [4]. Valid diagnostic tools such as the Autism Diagnostic Interview-Revised (ADI-R) in Chinese version play a significant role in diagnosing ASD in clinical settings [5]. The reduced subsets of ADI-R items and the Autism Diagnostic Observation Schedule (ADOS) may effectively distinguish ASD from other mental disorders, emphasizing the importance of accurate diagnostic instruments [6]. While the ADI-R and Second Edition of ADOS (ADOS-2) demonstrate a high degree of accuracy in research settings, their performance in clinical settings is less robust. Nonetheless, ADOS-2 appears to outperform ADI-R in diagnostic accuracy [7]. Nowadays, researchers are actively investigating diagnostic approaches for ASD utilizing electrophysiological and neuroimaging methodologies, especially functional Magnetic Resonance Imaging (fMRI). However, the temporal resolution of fMRI is constrained because of the circulatory system of the brain's delayed reaction and the inherent time limitations of the imaging process, rendering it less effective in capturing swift changes in brain activity [8].

Comparatively, EEG presents several advantages over fMRI, particularly its ability to study brain physiology across various age groups and developmental stages. Electroencephalography (EEG) and other electrophysiological techniques, like Magnetoencephalography (MEG), provide non-invasive methods to assess brain rhythms and dynamics, allowing for direct observation of neural activity with high temporal resolution [9]. Park et al. gathered information from medical records, psychological tests that measure intelligence quotient (IQ), and quantitative EEG (QEEG) during resting-state evaluations. Patients with each psychiatric condition and Healthy Controls (HCs) were divided into binary classification models using a combination of QEEG characteristics, such as Functional Connectivity (FC) and Power Spectrum Density (PSD) at frequency bands. Prediction performances were examined using Machine Learning (ML) techniques such as Support Vector Machine (SVM), random forest, and elastic net [10]. Major mental illnesses may be predicted by ML in EEG, which can also serve as an objective indicator of psychiatric diseases. In this research work, EEG was examined with classical ML and quantum ML for autism classification using the wavelet-based filterbank regularized common spatial pattern.

II. RELATED WORKS

Sinha et al. extracted features using Discrete Wavelet Transform (DWT) in the time and frequency domain after preprocessing the prerecorded EEG data using a digital filter. Neural networks, K-nearest neighbor (KNN), SVM, Linear Discriminant Analysis (LDA), and subspace KNN are some of the classifiers that utilize features for classification. Subspace KNN provides better accuracy for time-domain features [11]. Esqueda-Elizondo et al. calculated the band PSD to identify features related to attention detection and neurofeedback, including Alpha Relative Power (ARP), Theta Relative Power (TRP), Theta–Beta Ratio (TBR), Beta Relative Power (BRP), Theta/(Alpha+Beta), and Theta–Alpha Ratio (TAR). They employed these attributes to assess and train various machine-learning models. Multi-Layer Perceptron-Neural Network (MLP-NN) is used for classification [12]. Alotaibi and Maharatna determined the graph-theoretic parameters from three distinct methods based on a Phase-Locking Value (PLV) that have been quantitatively used to define the functional brain connection networks and were utilized as features in ML. Both the trial-averaged PLV technique and the cubic SVM were successful in autism classification [13]. In several studies, geometrical and graphical features are extracted to examine the complexity of EEG signals. For instance, Sadiq et al. explored the phase space dynamics of EEG signals to better visualize their chaotic and complex nature. They also identified 34 graphical features to decode the chaotic patterns of EEG signals [14]. Akbari et al. derived geometric features from the shapes of EEG signals. They selected relevant features using binary particle swarm optimization and employed SVM and KNN classifiers to differentiate between normal and depressed EEG signals [15]. Akbari et al. calculated geometrical features using the Poincaré pattern derived from DWT coefficients. Their findings suggest that the Poincaré pattern of seizure-free EEG exhibits more regular geometric shapes compared to that of seizure-related EEG [16].

Peketi and Dhok utilize Variational Mode Decomposition (VMD) to divide the EEG data into five distinct modes. For each mode, they extract thirty non-linear and linear features from both the time domain and the frequency domain. The dataset they selected faces a class imbalance issue, which they address using data augmentation through the synthetic minority oversampling technique. Subsequently, they compare three well-known machine learning classifiers. The best results were achieved using the fifth mode of VMD in conjunction with an SVM classifier with a fine Gaussian kernel [17]. Sadiq et al. introduced a framework that employs a multivariate variational mode decomposition method to extract multi-domain features and utilized wrapper and filter feature selection techniques. This framework is adaptable for classifying subject-dependent or independent brain-computer interface systems [18]. Subudhi et al. utilized Independent Component Analysis (ICA) to split these signals into additive subcomponents after preprocessing and low-pass filtering. Further investigation into significant nonlinear properties can

reveal non-biological phenomena and event-related possibilities. Then, SVM is employed for classification [19].

Baygin et al. extracted features from EEG signals using a one-dimensional local binary pattern. These features were then transformed into spectrogram images through a Short-Time Fourier Transform (STFT). For feature extraction, selection, and ranking, they employed the ReliefF algorithm along with a hybrid deep lightweight feature generator. To automate autism identification, shallow classifiers were utilized, with SVM achieving the highest accuracy among them [20]. Mohiud Din and Jayanthy utilized Continuous Wavelet Transform (CWT) to produce EEG signal scalograms. Deep Convolutional Neural Networks (CNN) that have already been trained, such as AlexNet, GoogLeNet, SqueezeNet, and MobileNet, were utilized to classify the scalograms that were acquired from the EEG signals of participants and to extract characteristics from the scalograms. In addition, the features were extracted using deep CNN and are classified using the Relevance Vector Machine (RVM) and SVM. GoogleNet, AlexNet, SqueezeNet, and MobileNet are deep CNNs used for categorization. SqueezeNet is more accurate at categorizing the scalograms that are produced from EEG data. Higher accuracy was achieved when scalogram features were retrieved using SqueezeNet and then fed into an SVM classifier [21]. Sadiq et al. analyzed scalograms, learning rates, features from untuned pre-trained models, pre-trained convolutional neural networks, and optimizers to improve the robustness of brain-computer interface systems. Their findings indicated that ShuffleNet achieved better accuracy at lower learning rates, resulting in optimal performance. However, the presence of noisy scalograms and features slightly reduced accuracy [22]. Tawhid et al. pre-processed the raw EEG data using a variety of methods, including normalization, filtering, and re-referencing. A STFT is then utilized to convert the EEG signal into two-dimensional (2)-D) images. Textural features are then retrieved, Principal Component Analysis (PCA) is used to select significant features, and the results are trained into an SVM classifier [23] and three distinct models of convolutional neural networks. CNN model surpasses previous approaches and achieves greater accuracy compared to the SVM model [24]. A few studies utilized the Multiscale Principal Component Analysis (MSPCA) to remove the noise of EEG data. Sadiq et al. developed an automated Multivariate Empirical Wavelet Transform (MEWT) algorithm. The algorithm uses an MSPCA method for robustness against noise, an automated channel selection approach, a method for sub-band alignment, and a reliable feature selection technique based on correlation. The algorithm also provides better classification accuracy for subject-specific cases, subject-independent, and subjects with limited training data [25].

Sadiq et al. utilize methods such as MSPCA, Improved Empirical Fourier Decomposition (IEFD), Empirical Fourier Decomposition (EFD), and feedforward neural network classifiers to enhance brain-computer interface systems for classifying motor imagery EEG tasks. Their framework increases classification accuracy by examining various combinations of signal decomposition and feature selection methods, validating the results through performance metrics and statistical analysis [26]. Similarly, Yu et al. developed an automated framework for detecting motor and mental imagery (MeI) EEG tasks [27]. Sadiq et al. utilized MSPCA to obtain noise-reduced EEG signals. After denoising, the signals were decomposed into various modes using empirical wavelet transform. This process was followed by two-dimensional modeling and the extraction of geometric features. Finally, both cascade-forward and feedforward neural networks were employed for motor imagery classification tasks [28].

Alturki et al. utilized ICA to remove artifacts from EEG datasets. They extracted EEG features using energy, band power, and entropy in combination with Common Spatial Pattern (CSP) techniques. Four classification methods were employed in the study such as Artificial Neural Networks (ANN), KNN, SVM, and LDA. The best performance was achieved by combining CSP, Local Binary Pattern, and KNN [29]. Antony et al. utilized Online Recursive Independent Component Analysis (ORICA)-CSP to extract features. ORICA-CSP approach is combined with the Adaptive Support Vector Machine (A-SVM) for classification [30]. Hwang et al. employed Filter Bank CSP (FBCSP), which is based on overlapping bands, to extract specific spatial features from the subject. In this method, time-varying EEG signal data is generated using a sliding window technique [31]. Mohamed et al. employed Scaled and warped CSP (SWCSP) in the data. To identify the most discriminating SW-CSP filters, the Fisher's score method is utilized [32]. To extract the feature, Moufassih et al. used Boosted Tangent Space Mapping (BTSM) and Multi-Band CSP (MBCSP). An automatic feature selection algorithm reduces high-dimensionality space. The class of the Motor Imagery trial is determined using the Logit Boost classifier [33].

Rithwik et al. employed Filter bank-based Spatially Regularized CSP (FBSRCSP) method to decode bidirectional hand movements. Regularization techniques enhance direction discriminability and use LDA for classification accuracy. The FBSRCSP offers the better average classification accuracy [34]. Shang et al. divide EEG signal into multiple frequency bands using enhanced wavelet threshold algorithm, and constructing spatial filters to extract EEG signal characteristics. The SVM optimized with a genetic algorithm, is used for EEG signal classification [35]. Wang et al. utilized Geodesic Filtering CSP (GFCSP) and filter-bank Feature Weighted SVM (FWSVM) for the classification of motor imagery [36]. Wang et al. extracted the Event-Related Desynchronization (ERD) and Movement-Related Cortical Potential (MRCP) features using Common Spatial Pattern and Discriminative canonical pattern matching (DCPM). Fisher Discriminant Analysis (FDA) classifier is utilized for classification [37]. Zahid et al. employed the Maximum-A-Posteriori

(MAP)-CSP framework to classify multiple motor imagery tasks. They filtered pre-processed EEG signals in the mu and beta brainwave frequency range, then selected the most crucial features, and un-regularized LDA was utilized for classification [38]. Zhang et al. utilized Common spatial pattern and Tikhonovo regularisation CSP (TRCSP) spatial filters for feature extraction, with SVM and LDA for classification. The TRCSP-SVM method demonstrated significantly better performance [39]. Zhang et al. utilized TRCSP to extract features based on temporal-spatial- frequency. The method extracts diverse feature subsets, uses the base model, such as the Least Absolute Shrinkage and Selection Operator (LASSO), and uses diverse models for ensemble model construction [40]. Lins et al. preprocessed the EEG signals, extracting Higuchi fractal dimension, complexity, and mobility features. They trained Quantum ML (QML) models using quantum circuit layers and compared the results [41]. Aksoy et al. employed wavelet transformations on EEG data and extracted statistical features, which were subsequently dimension-reduced using PCA. Dimension-reduced data is exposed to conventional classification techniques, after which it is translated into qubit format using feature maps, and QML models are used for classification [42].

Enad and Mohammed employed PCA, min-max normalization, and recursive feature elimination to preprocess the dataset. They compared traditional classifiers, such as ANN and SVM, with a QML approach. Two distinct QML classification methods, Quantum Support Vector Machines (QSVM) and Quantum Neural Network (QNN), were analyzed. The bagging-QSVM model showed significantly better performance [43]. Garg et al. utilized Quantum SVM to classify emotions on the benchmark dataset [44]. Accuracy and execution speed of QSVM classification based on selecting the correct quantum feature map for complex datasets [45]. Stochastic gradient descent (SGD) has been shown in numerous theoretical works in the deep learning regime to be an effective tool for learning models to escape saddle points efficiently. Although Qian et al. used SGD with the correct batch size to slightly enhance QNN optimization, other regularization techniques, such as weight decay, do not improve the trainability of QNNs [46].

A. RESEARCH GAP

The work proposed addresses the following research gaps in ASD and Typically Developed (TD) classification.

1) An objective method for diagnosing ASD requires a higher number of EEG channels to facilitate a thorough analysis of neural activity.
2) Enhancing accuracy in distinguishing between ASD and TD over time, frequency, or time-frequency domain features requires improvement when utilizing the minimum number of channels.
3) The accuracy of QSVM relies on the selection of an appropriate quantum-based feature map.
4) The accuracy of QNN depends on both the selection of an appropriate combination of quantum feature maps and the optimization algorithm employed.

B. RESEARCH CONTRIBUTIONS

The key contributions of this research are as follows:

1) Identify the optimal combination of two electrodes for ASD detection.
2) Enhance discrimination between ASD and TD by extracting spatial patterns from EEG signals using wavelet–based filterbank regularized CSP.
3) Utilize amplitude embedding to improve the classification performance of QSVM for autism classification.
4) Utilize the combination of amplitude embedding quantum feature map and the SGD optimization algorithm to enhance the performance of QNN.

III. MATERIALS AND METHODS

The proposed approach is divided into 5 main steps: (1) Data acquisition and preprocessed data, (2) wavelet-based Filter Bank regularized Common Spatial Pattern, (3) Feature extraction, (4) Feature selection, and (5) Machine learning methods. The overall proposed approach block diagram is shown in Figure 1.

A. DATA ACQUISITION AND PREPROCESSING

Ten ASD children and ten children with TD, ages between five and seven, participated in the research study. Using the Fifth Edition of the Diagnostic and Statistical Manual of Mental Disorders (DSM V) evaluation, the individual's cognitive abilities were assessed. The research study received prior approval from the Institutional Review Board and Ethics Committee of the Sri Ramachandra Institute of Higher Education and Research (SRIHER). The parents or guardians of the children gave their informed consent before data collection. The ''Indian Scale for Assessment of Autism (ISAA)'' was used to diagnose autism, classifying children as having autism if their score was 70 or more and as not having autism if it was less than 70. Children with ASD were trained to focus on the video while the data was being collected. The video's visual screen was placed 45 centimeters away. During visual screen follow-up sessions of training, sometimes their favorite cartoon videos are presented.

An SRIHER-affiliated occupational therapist suggested these particular videos. Ag/AgCl electrodes were applied to the scalp during the EEG signal acquisition process, and good conduction was ensured via conductive gel and tape. Following the 10-20 International Standard, three electrodes of raw EEG signals were acquired at a 500 Hz sample rate. In this research, EEG signals from the C3, C4, and Cz electrodes were utilized. The Nihon Kohden Neurofax MEB9000 version 05-81 at a sensitivity of 7 μV was utilized to record EEG signals. Preprocessing was conducted using their software tools. Low-pass and high-pass filters with a cutoff frequency range of 0.53 to 70 Hz were applied, fol-

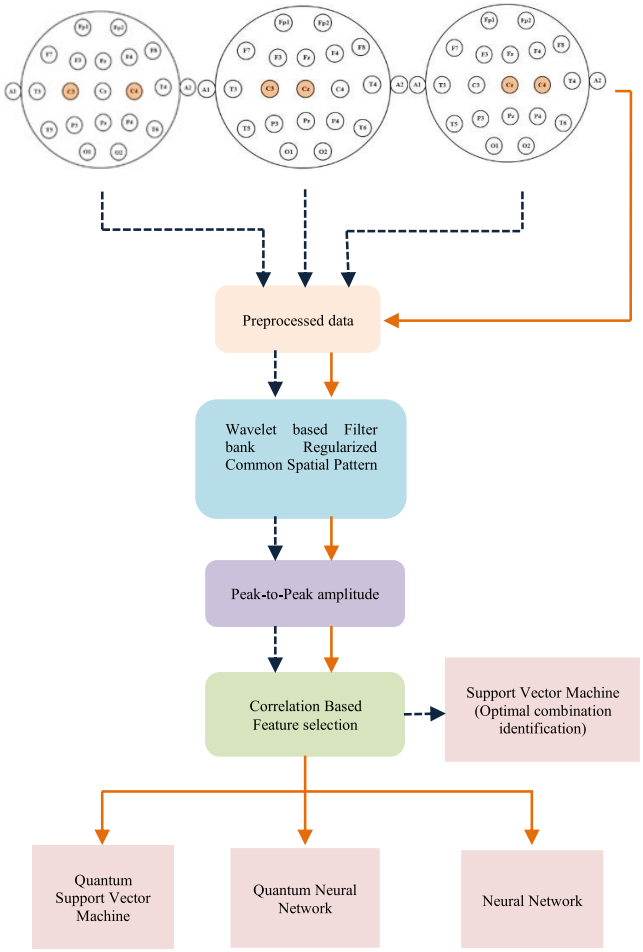

FIGURE 1. Block diagram of the overall proposed approach.

lowed by a 50 Hz notch filter. The ocular artifacts in the EEG signals were eliminated using a thresholding method. The threshold was determined based on the average amplitude of the eye blink signal. To establish this, the eye blink signal was recorded for 10 seconds during both eye-open and eye-close events. Signals exceeding this threshold were excluded, and the remaining data was used for further analysis. Muscular artifacts typically appear as sharp, high-frequency bursts (spikes) or periodic activity in the 20–70 Hz range in the obtained EEG data. These artifacts are visually inspected and removed manually by an expert.

B. WAVELET-BASED FILTER BANK REGULARIZED COMMON SPATIAL PATTERN

EEG signals are non-stationary; therefore, the Fourier transform does not help evaluate EEG signals. The DWT offers a method to quantitatively analyze the multiple frequency bands of EEG brain waves. In this research work, wavelet decomposition is applied to an EEG signal using the Daubechies 4 (db4) wavelet at level 3, decomposing it into several layers that represent different frequency components and details. Filters are then applied to the wavelet detail coefficients to emphasize specific frequency components that are relevant for classification or analysis. The modified wavelet coefficients are used to reconstruct the decomposed signal, providing a transformed representation of the EEG data. This reconstructed data is subsequently processed through a Butterworth filter bank for signal filtration and divided into six frequency sub-bands (8-12 Hz, 12-16 Hz, 16-20 Hz, 20-24 Hz, 24-28 Hz, and 28-32 Hz). Finally, spatial filtering is performed using the wavelet-based filterbank regularized CSP approach, which aims to minimize the variance within the other class while maximizing the variance within one class.

Given a single trail matrix $E_{k,i} \in X^{m \times s}$ where m represents the number of electrodes and s is the number of data points, the mean normalized covariance matrix is determined by Eq. (1).

$$C_{ij} = \frac{1}{N} \sum_{i=1}^{N} \frac{E_{k,i} E_{k,i}^T}{trace\left(E_{k,i} E_{k,i}^T\right)} \tag{1}$$

where N represents the number of trails that follow for each class, i = 1, …, n is the segment that corresponds to class i, and k is the class type (either ASD or TD). Tikhonov regularization should be applied to each class's covariance matrix.

The composite covariance matrix is generated by taking the mean of the regularized covariance matrices for each class. The generalized eigenvalue decomposition method is applied to the composite or average covariance matrix to obtain the corresponding eigenvalues and eigenvectors. Using the eigenvalues of the composite matrix, the whitening matrix P was constructed according to Eq. (2) to normalize the variances to a value of one.

$$P = \sqrt{\lambda}^{-1} \times V^T \tag{2}$$

The generalized eigenvalue decomposition is applied to each class S matrix, which is a combination of matrix multiplication of the transpose of the whiten matrix, the covariance matrix for each class, and the whiten matrix to obtain the eigenvalues and associated eigenvectors. The eigenvector B and eigenvalue λ of the S matrices are determined for each class. The projection matrix is then acquired using Eq. (3).

$$W = B^T P \tag{3}$$

The Projection matrix (W) is derived from the transpose of eigenvector (B) and the whitened matrix (P). The CSP algorithm yields the projection matrix W, which strives to maximize the variance ratio between two distinct classes of data. The W matrix's initial row, which has the most significant eigenvalue, and the last row, which has the smallest eigenvalue, is used in this way to create the most significant spatial pattern. In Equation 4, the EEG signal is recovered.

$$X = W^{-1} Z \tag{4}$$

The spatial pattern is represented by each column of the W^{-1}, which is regarded as an EEG distribution vector. Consider X to be a $m \times s$ matrix, where m represents the number

of EEG electrodes and s represents the number of data points. The rows of the CSP projection matrix W are arranged to represent spatial filters, and the columns to represent common spatial patterns. The process of calculating W for every class entails increasing the ratio between the mean covariance matrices of those classes.

C. FEATURE EXTRACTION AND SELECTION

In this work, peak-to-peak amplitude is used as a feature for classification. The feature vector (X_i) is calculated from Z (i.e. Z_i where i = [1, . . . , d]). The calculation of X_i using the log peak-to-peak amplitude method is as follows in Eq. (5).

$$X_i = \log\left(\frac{ptp\,(Z_i)}{\sum_{i=1}^{d} ptp\,(Z_i)}\right) \tag{5}$$

When predicting a linear relationship between the signals of interest, the correlation coefficient is useful. It is very good at expressing linear dependencies and gives a clear understanding of the strength and direction of the relationship. Therefore, it is utilized in this particular scenario to compute the Pearson correlation coefficients between each feature in the input feature matrix X and the target variable y. Features with high correlations with the target variable are indeed more informative for prediction. The resultant r value is between −1 and 1. SelectKBest is a more comprehensive approach since it allows the feature selection process to be performed using an extra scoring function parameter.

D. SUPPORT VECTOR MACHINE

For classification tasks, SVM is a widely used supervised machine learning method. Although many possible decision boundaries could divide the classes, its primary goal is to create an optimal hyperplane, or decision boundary, within an n-dimensional space to effectively separate different classes for accurate classification. The features in the dataset determine the dimensions of the hyperplane. The hyperplane will be a straight line if the dataset only has two features. SVMs offer various kernel functions, including the polynomial function, Radial Basis Function (RBF), and linear function. This research employs the RBF kernel and is calculated using Eq. (6).

$$K\,(X_1, X_2) = exp\left(-\frac{\|X_1 - X_2\|^2}{2\sigma^2}\right) \tag{6}$$

where σ is the variance and hyperparameter, $\|X_1 - X_2\|$ is the Euclidean Distance between two points X_1 and X_2.

E. NEURAL NETWORK

Neural networks (NN) process complex data to detect patterns, similar to the human brain. They are composed of three layers: Input, Hidden, and Output. Each neuron receives information, performs calculations, and passes the results to the next layer. The hidden layers transform the input data, with weights determining the influence on the output. Bias represents the deviation from the intended value; low bias indicates more assumptions, while high bias indicates fewer assumptions, which can impact the accuracy of the model. The linear combination of the inputs is given in Eq. (7).

$$Z = xW + b \tag{7}$$

where x is the input vector, W is the weight matrix, and b is the bias vector. The first and hidden layer output is calculated with the ReLU activation function as follows in Eq. (8).

$$a = ReLU\,(z) \tag{8}$$

The final layer output is calculated with the sigmoid activation function. The sigmoid activation function is calculated using Eq. (9).

$$sigmoid\,(Z) = \frac{1}{1 + e^{-Z}} \tag{9}$$

Binary cross-entropy loss function is calculated using Eq. (10).

$$loss = -\frac{1}{N}\sum_{i=1}^{N} y_i . \log\,(p\,(y_i)) + (1 - y_i)\,.\log\,(1 - p\,(y_i)) \tag{10}$$

where y is considered as a label and p(y) is considered as a predicted probability of the data point being the desired class for all N data points.

F. QUANTUM MACHINE LEARNING

Recently, there has been significant growth in the fields of ML and Deep Learning (DL). However, these models require millions of parameters to learn as the number of features rises, which results in inefficient training and substantial computational burdens. Quantum computers have demonstrated the capability to address these issues by computing several states concurrently using existing technologies. They utilize three quantum physics properties: entanglement, superposition, and interference. Due to quantum physics properties, qubits (the fundamental units of quantum computers) maintain strong correlations even over large distances (entanglement), exist in several states at once (superposition), and be influenced to favor specific outcomes (interference). This inherent potential of quantum computing brings the research community closer to achieving Artificial General Intelligence. Quantum-enhanced machine learning is a technique designed to improve traditional machine learning algorithms using quantum computing. This approach is a subfield of quantum information processing [47]. For instance, a classifier based on Quantum Machine Learning utilizing a Variational Quantum Circuit (VQC) with adjustable hyperparameters. The three primary parts of this quantum circuit are an encoder, which creates quantum states from input data, a decoder, which creates output states, and an evaluator, which compares the circuit's output values with the associated input labels. Pauli-Z operators are used in the evaluation, and the average evaluated value is used to improve statistical correctness. By optimizing the cost function, the quantum gates of the decoder are parameterized to simulate the input training data [48].

1) QUANTUM SUPPORT VECTOR MACHINE

SVM classifies difficult datasets using the "kernel trick", which projects input data points into a high-dimensional space and facilitates the solution to non-linear separable issues. Currently, there are several kernel functions utilized, which can be computationally expensive and inefficient. So Quantum Kernel is used. Quantum kernels use quantum mechanics to improve feature vector mapping. Quantum Kernel-Based Machine Learning, incorporating QSVM, is revolutionizing data analysis and classification. By integrating quantum principles, these innovations unlock unprecedented computational capabilities, outperforming classical methods in various applications. Quantum kernel machine learning relies on using quantum feature maps to carry out the kernel trick. Here, a quantum feature map transforms a classical feature x into a point in Hilbert space, yielding the quantum kernel. ϕ(x). It is mathematically illustrated by Eq. (11).

$$K_{ij} = \left|\left\langle \phi\left(\vec{x}_i\right) \mid \phi\left(\vec{x}_j\right)\right\rangle\right|^2 \tag{11}$$

where K_{ij} is the kernel matrix, $\phi(x)$ is the quantum feature map, x_i, and x_j are n-dimensional inputs, and $|\langle a \mid b\rangle|^2$ denotes the two quantum states, a and b, overlap. Figure 2. Depicts the block diagram of the QSVM.

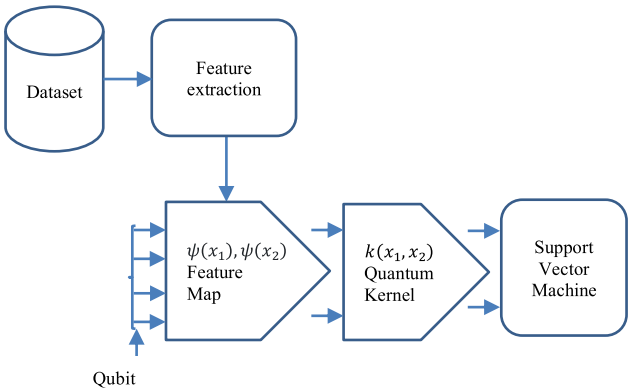

FIGURE 2. Block diagram of the Quantum SVM.

2) QUANTUM NEURAL NETWORK

The hidden layers in the neural network are replaced by a quantum-based layer to create a QNN. The inputs for the quantum layer of the neural network will be gathered from the outputs of the preceding layer. After that, the measurement observable from the quantum layer was gathered and used as input for the subsequent output layer. Figure 3. depicts the block diagram of QNN with two quantum layer.

IV. RESULT ANALYSIS

This section discusses the environmental setup utilized for the research work, the analysis of different Combinations of electrodes, and the analysis of quantum machine learning techniques.

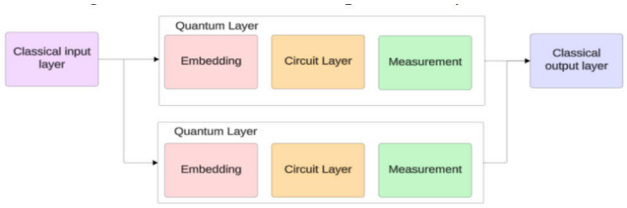

FIGURE 3. Block diagram of the quantum neural network.

A. ENVIRONMENTAL SETUP

Colab was used along with Python 3.7.12. The dataset was divided with an 80/20 split using the train split algorithm, ensuring subject independence to prevent any potential data leakage between the training and testing sets. Specifically, data from each subject was kept exclusive to either the training or testing set. Scikit-learn were used to carry out the standardization processes. Numpy, Scipy, and Pandas were used to read and process the data. Pennylane and Sklearn libraries are utilized for classifiers. Accuracy, specificity, precision, F1 score, and sensitivity were used to gauge the performance of the proposed approach.

B. ANALYSIS OF DIFFERENT COMBINATION OF ELECTRODES

Initially, various combinations of the electrodes were examined to assess their impact on accuracy. Combining C3 and C4 electrodes yielded an accuracy of 85.1%. Similarly, combining C3 and Cz electrodes produced an accuracy of 91.2%, while combining C4 and Cz electrodes resulted in an accuracy of 93.9%. Upon analyzing these combinations, it was observed that either C3 or C4, when combined with the midline electrode Cz, achieved the highest accuracy. Specifically, the combination of C4 with Cz consistently demonstrated better accuracy across SVM with an RBF kernel. Figure 4 depicts the performance metrics of three different combinations of electrodes with an SVM classifier.

The input layer, one intermediate layer, and the output layer of the NN model were used to train the combination of the C4 and Cz electrodes. The model employs the Adam optimizer for optimization and the binary cross-entropy loss function. Fig. 4. depicts the performance metrics for the combination of the C4 and Cz using SVM. Table 1. shown the evaluation of performance metrics for SVM and Neural Networks with C4-Cz Electrode Combination.

TABLE 1. Performance metrics for the C4-Cz electrode combination using SVM and neural networks.

Method	Accuracy (%)	Precision (%)	Sensitivity (%)	Specificity (%)	F1-Score (%)
SVM	93.85	93.85	94.73	92.98	93.93
NN	90.9	89.6	91.5	90.4	90.5

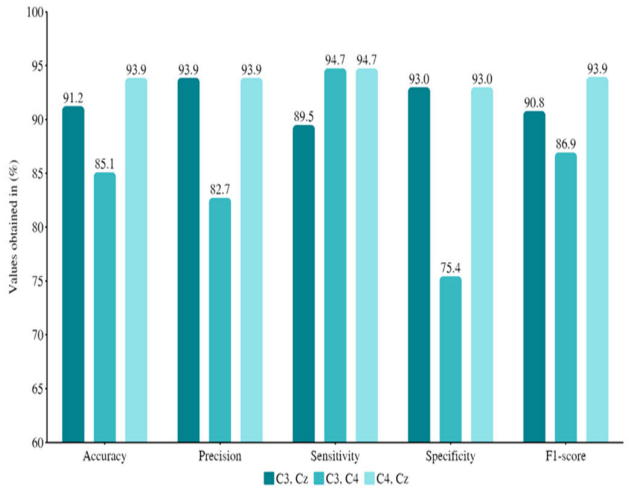

FIGURE 4. Performance metrics of the three different combinations of electrodes with SVM classifier.

C. ANALYSIS OF QUANTUM MACHINE LEARNING

This section presents an analysis of QSVM and QNN. PennyLane is an open-source, cross-platform Python library that supports a wide array of tasks in quantum computing, quantum chemistry, and quantum machine learning. Train the quantum circuits with their different programming capabilities for quantum computers, which are designed to work smoothly with hardware, simulators, and classical machine-learning libraries.

1) QUANTUM SUPPORT VECTOR MACHINE ANALYSIS

A quantum kernel encodes two classical input vectors, x_1, and x_2, into quantum states using amplitude embedding. It then applies the adjoint of the embedding for x_2 to reverse its effect and measure the similarity between the quantum states of x_1 and x_2. This similarity is determined by calculating the expectation value of a Hermitian projector, yielding the quantum kernel value. The kernel matrix, a symmetric matrix representing pairwise quantum kernel evaluations between data points, is integral to the process. SVM is a supervised machine learning algorithm utilized for classification tasks, relying on a quantum kernel matrix to operate in a higher dimensional space. Figure 5 depicts the quantum state vector obtained by amplitude embedding for the classical feature of the EEG signal.

```
Quantum State Vector:
[0.00240486+0.j 0.01442916+0.j 0.00721458+0.j 0.01923889+0.j
 0.2885833 +0.j 0.2885833 +0.j 0.2885833 +0.j 0.2885833 +0.j
 0.2885833 +0.j 0.2885833 +0.j 0.2885833 +0.j 0.2885833 +0.j
 0.2885833 +0.j 0.2885833 +0.j 0.2885833 +0.j 0.2885833 +0.j]
```

FIGURE 5. Quantum state vector obtained after amplitude embedding.

The Bloch sphere is a geometric representation of qubit states as points on the surface of a unit sphere. To compute the Bloch sphere for a specific qubit, the reduced density matrix is required, which is obtained by tracing out the other qubits from the full-density matrix ($2^{n\_qubits} \times 2^{n\_qubits}$) of the system. The full density matrix is calculated using the outer product of the state vector with its conjugate transpose, encapsulating all information about the quantum system, including both pure and mixed states. The total number of possible states for the system is 2^{n_qubits}, where *n_qubits* refers to the number of qubits in the system. In this research, four qubits are utilized. The reduced density matrix is computed by iterating over all possible basis states i and j of the entire quantum system. If the state of qubit at indices i and j is the same, the corresponding element of the full density matrix is added to the reduced density matrix.

The reduced density matrix is then used to calculate the Bloch vector, which geometrically represents the quantum state of the qubit on the Bloch sphere. The Bloch vector consists of three components: $x, y, andz$. The x-component is calculated from the real part of the sum of the off-diagonal elements, providing information about the coherence between the $|0\rangle$ and $|1\rangle$ states. The y-component is derived from the imaginary part of the difference between the off-diagonal elements, indicating coherence in a different orientation on the Bloch sphere. The z-component is determined from the diagonal elements of the reduced density matrix, representing the populations of the $|0\rangle$ and $|1\rangle$ states. Padding with a constant value of 12 is utilized during the amplitude embedding process. Include the Hadamard gates to all qubits to create superposition in the Bloch sphere. Figure 6. Depicts the Bloch sphere vector representation of the individual qubit.

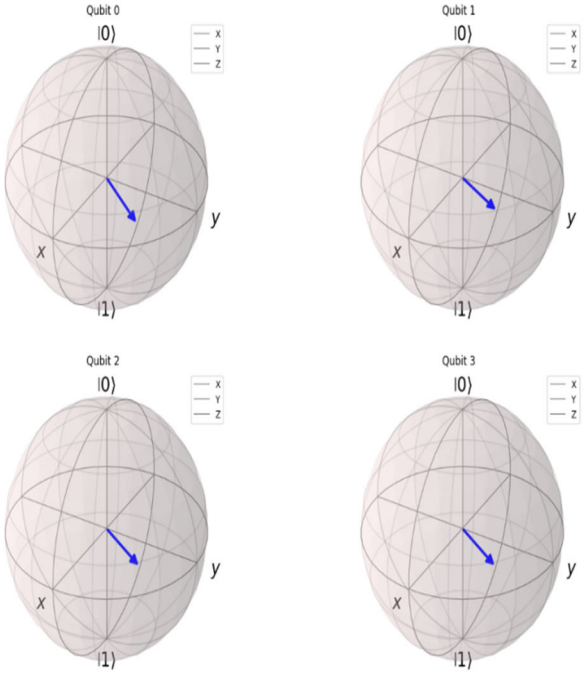

FIGURE 6. Bloch sphere representation of Qubit0, Qubit1, Qubit2, Qubit3.

2) QUANTUM NEURAL NETWORK ANALYSIS

The QNN model begins with 4-dimensional input data, which is fed into the initial classical layer. During training, 20% of the neurons in this layer are randomly set to zero, courtesy of the dropout layer. The outputs from this classical layer are then directed towards two separate 2-qubit quantum layers, where quantum computations process the classical information. Subsequently, the outputs from these quantum layers are merged. The combined output is passed to the final classical layer, consisting of 2 neurons. This final classical layer produces the ultimate output. Quantum layers, obtained via QNodes, can be converted into keras layers using the keras Layer class from the qnn module. To embed the classical data into a quantum feature map, amplitude embedding is utilized.

The weights argument of the QNode is trainable and possesses a shape given by several layers and several qubits, which is passed to BasicEntangler Layers. Finally, the QNode returns expectation values for the Pauli-Z observable, which holds significant importance in quantum mechanics and quantum computing. It offers a means to investigate and manipulate quantum states and their properties. Figure 7. depicts the accuracy and loss metrics during training and validation for QNN. Table 2 shows the comparison of performance metrics for quantum machine learning using the combination of C4 and Cz.

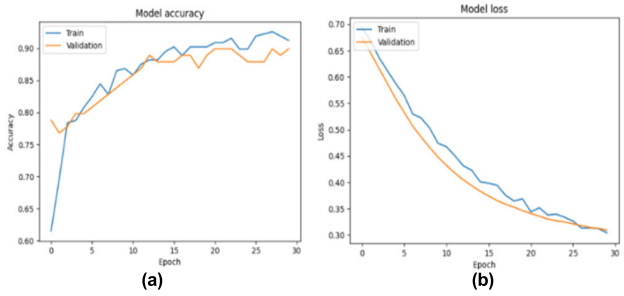

FIGURE 7. Training and validation metrics for Quantum Neural Network (QNN) (a) Accuracy (b) Loss.

TABLE 2. Comparison of performance metrics of the quantum machine learning for the combination of C4 and Cz.

Method	Accuracy (%)	Precision (%)	Sensitivity (%)	Specificity (%)	F1-Score (%)
QSVM	94.73	93.94	98.24	91.22	94.41
QNN	93.94	92.45	96.08	91.67	94.23

D. EFFECT OF THE COMBINATION OF FREQUENCY AND TIME-FREQUENCY DOMAIN FEATURES

Conventional methods like the STFT and wavelet transform are commonly used for time-frequency analysis. However, both face challenges related to resolution. The STFT uses a fixed-sized window, which compromises the ability to balance time and frequency resolution. The Wavelet Transform, on the other hand, offers multi-resolution analysis but lacks a direct and explicit alignment with the Fourier spectrum, which can make interpretation less intuitive. The Stockwell Transform (ST) merges the benefits of both the STFT and Wavelet Transform, overcoming their limitations. The ST is characterized by its use of a scalable, moving Gaussian window that adapts its resolution depending on the frequency of the signal. This unique feature allows the ST to provide frequency-dependent resolution, offering higher time resolution for high-frequency components and better frequency resolution for low-frequency components.

Moreover, the S-transform maintains a direct and explicit relationship with the Fourier spectrum, providing a more flexible and informative tool for time-frequency analysis. As a result, the ST is particularly effective for analyzing non-stationary signals, where frequency content changes over time. In this research work, the ST is used to decompose a signal into its time-frequency components, focusing on a specific frequency range defined by minimum frequency and maximum frequency. The frequency range is first converted into corresponding indices based on the sampling frequency (fs) and signal length. The ST is then computed, and its components within the target frequency band are extracted. The mean absolute values of the Stockwell Transform and peak frequencies (Welch method) for each signal across six subbands for each EEG segment are extracted. The average values across two signals for each subband are then calculated. The peak-to-peak amplitude values extracted previously are combined with frequency-domain and time-frequency domain features. The feature vector, comprising a total of 24 features per EEG segment, is then generated. Correlation-based feature selection was applied to select the top 4 most relevant features for classification, which helped to optimize the model's performance. Figure 8. Depicts the performance metrics of different feature combinations with QSVM for autism classification.

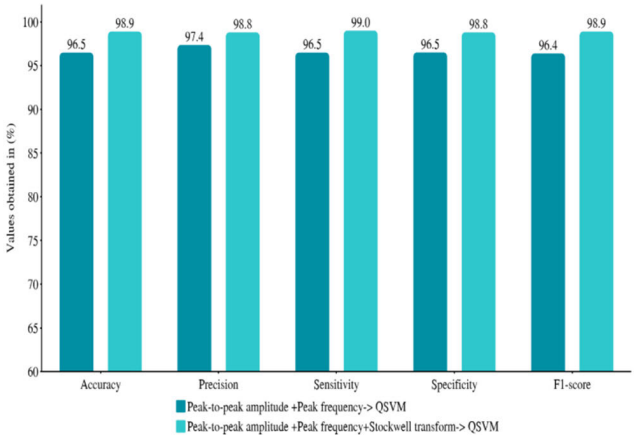

FIGURE 8. Performance metrics of different feature combinations with QSVM.

V. DISCUSSION

The objective of this research is to identify ASD and TD individuals using a minimal number of EEG channels. Different combinations of three electrode placements, specifically

TABLE 3. Comparison of the proposed system with existing systems.

Source	Method	Number of channels	Classifier	Accuracy (%)
Tawhid et al. [23]	Texture-based features extracted from spectrogram images	16 channels	SVM	95.25
Baygin et al. [20]	Features are derived from spectrogram images using the pre-trained models ShuffleNet, MobileNetV2, and SqueezeNet.	64 channels	SVM	96.44
Sinha et al. [11]	Alpha, beta, delta, theta, and gamma, along with mean, variance, standard deviation, kurtosis, skewness, and Shannon entropy features, were extracted.	16 channels	Subspace KNN	92.8
Proposed approach	The integration of a wavelet-based regularized filter bank common spatial pattern with peak-to-peak amplitude, Stockwell transform, and peak frequencies features.	2 channels	QSVM	98.24

(C3, C4), (C3, Cz), and (C4, Cz), were evaluated as inputs to the system. Initially, the EEG signals are processed using wavelet transform with the Daubechies 4 (db4) wavelet at level 4. The wavelet transform breaks down a signal into distinct frequency components, which involves Approximation Coefficients representing low-frequency (coarse) details of the signal. Detail Coefficients are capturing high-frequency (fine) details of the signal. Filtering and Reconstruction After decomposition, filters are applied to the wavelet detail coefficients obtained at various levels. Post-filtering, the modified wavelet coefficients are used to reconstruct the signal. The reconstructed signal undergoes processing with a filterbank Tikhonov regularized CSP to enhance discrimination between two classes using spatial features of the signal. The spatially filtered signal is then used to extract peak-to-peak amplitude features with a vector length of 12 for the EEG segment, and correlation-based feature selection selects the top 4 features. An SVM classifier is employed to classify the EEG signal. Among the tested combinations (C4, Cz), better accuracy was achieved. When trained on a neural network, the combination (C4, Cz) attained an accuracy of 90.9%. The research work incorporated quantum machine learning techniques to enhance classification performance. Feature maps are crucial to quantum machine learning because they convert classical data to quantum data.

In this work, a quantum kernel with amplitude embedding was applied instead of a classical kernel in the SVM, resulting in an accuracy of 94.7%. The neural network architecture was modified by incorporating two 2-qubit quantum layers with amplitude embedding instead of traditional hidden layers. This approach achieved an accuracy of 93.9% with the SGD optimizer. The incorporation of quantum machine learning techniques further improved the performance, showcasing the potential of quantum approaches in enhancing classification accuracy beyond classical methods. Incorporating additional features, peak frequency and Stockwell transform with peak-to-peak amplitude, provides further enhanced accuracy when it is classified using QSVM. Unlike previous methods, which focus solely on time, frequency, and time-frequency domain information with machine learning and deep learning, our approach integrates time, frequency, and time-frequency domain information with spatial information and quantum machine learning. This allows for better classification and improves accuracy compared to traditional approaches. Table 3 presents a comparison between the proposed system and existing systems.

VI. CONCLUSION

This study explores the challenge of diagnosing ASD using EEG data and advanced machine learning techniques. The goal was to identify the best combination of EEG electrodes to enhance classification performance. EEG signals were processed, and three electrode pairs—C3-C4, C3-Cz, and C4-Cz—were analyzed. Among these, the C4-Cz pair, combined with an SVM classifier achieved the highest classification accuracy and was selected for detailed analysis. Quantum machine learning methods, including QSVM and QNN with amplitude embedding, were then applied. By incorporating additional features such as peak frequency, Stockwell transform coefficients, and peak-to-peak amplitude, QSVM achieved an accuracy of 98.9%. The electrode combinations were compared based on their classification performance, leading to the selection of the most effective pair for analysis. Future research could expand the scope to include larger and more diverse participant groups. Investigating self-supervised learning approaches for ASD detection using Magnetoencephalography (MEG) signals and applying neural structured learning with Riemannian features are promising future directions for advancing this field.

ACKNOWLEDGMENT

The authors would like to acknowledge Sri Ramachandra Medical College and Research Institute, India, for providing the datasets used in this study.

REFERENCES

[1] M. J. Maenner, "Prevalence and characteristics of autism spectrum disorder among children aged 8 years—Autism and developmental disabilities monitoring network, 11 sites, United States, 2020," *MMWR. Surveill. Summaries*, vol. 72, no. 2, pp. 1–14, Mar. 2023, doi: 10.15585/mmwr.ss7202a1.

[2] S. H. Zuvekas, S. D. Grosse, T. A. Lavelle, M. J. Maenner, P. Dietz, and X. Ji, "Healthcare costs of pediatric autism spectrum disorder in the United States, 2003–2015," *J. Autism Develop. Disorders*, vol. 51, pp. 2950–2958, Oct. 2020, doi: 10.1007/s10803-020-04704-z.

[3] K. Marta, C.-Ł. Justyna, S. Marta, L. Jerzy, P.-B. Justyna, B.-Z. Agnieszka, and O. Danuta, "Selected methods of therapeutic interactions with people with mild symptoms of autism spectrum disorder," *Frontiers Psychiatry*, vol. 13, Jul. 2022, Art. no. 942218, doi: 10.3389/fpsyt.2022.942218.

[4] P. Singhi and P. Malhi, "Early diagnosis of autism spectrum disorder: What the pediatricians should know," *Indian J. Pediatrics*, vol. 90, no. 4, pp. 364–368, Oct. 2022, doi: 10.1007/s12098-022-04363-1.

[5] C.-F. Huang, Y.-S. Lin, Y.-N. Chiu, S. S.-F. Gau, V. C.-H. Chen, C.-F. Lin, Y.-H. Hsieh, W.-S. Liu, H.-L. Chan, and Y.-Y. Wu, "Validation of the Chinese version of the autism diagnostic interview-revised in autism spectrum disorder," *Neuropsychiatric Disease Treatment*, vol. 18, pp. 327–339, Feb. 2022, doi: 10.2147/ndt.s345568.

[6] I. Kamp-Becker, J. Tauscher, N. Wolff, C. Küpper, L. Poustka, S. Roepke, V. Roessner, D. Heider, and S. Stroth, "Is the combination of ADOS and ADI-R necessary to classify ASD? Rethinking the 'gold standard' in diagnosing ASD," *Frontiers Psychiatry*, vol. 12, Aug. 2021, Art. no. 727308, doi: 10.3389/fpsyt.2021.727308.

[7] J. B. Lebersfeld, M. Swanson, C. D. Clesi, and S. E. O'Kelley, "Systematic review and meta-analysis of the clinical utility of the ADOS-2 and the ADI-R in diagnosing autism spectrum disorders in children," *J. Autism Develop. Disorders*, vol. 51, no. 11, pp. 4101–4114, Jan. 2021, doi: 10.1007/s10803-020-04839-z.

[8] M. Khodatars, A. Shoeibi, D. Sadeghi, N. Ghaasemi, M. Jafari, P. Moridian, A. Khadem, R. Alizadehsani, A. Zare, Y. Kong, A. Khosravi, S. Nahavandi, S. Hussain, U. R. Acharya, and M. Berk, "Deep learning for neuroimaging-based diagnosis and rehabilitation of autism spectrum disorder: A review," *Comput. Biol. Med.*, vol. 139, Dec. 2021, Art. no. 104949, doi: 10.1016/j.compbiomed.2021.104949.

[9] P. Garcés, "Resting state EEG power spectrum and functional connectivity in autism: A cross-sectional analysis," *Mol. Autism*, vol. 13, no. 1, May 2022, Art. no. 22, doi: 10.1186/s13229-022-00500-x.

[10] S. M. Park, B. Jeong, D. Y. Oh, C.-H. Choi, H. Y. Jung, J.-Y. Lee, D. Lee, and J.-S. Choi, "Identification of major psychiatric disorders from resting-state electroencephalography using a machine learning approach," *Frontiers Psychiatry*, vol. 12, Aug. 2021, Art. no. 707581, doi: 10.3389/fpsyt.2021.707581.

[11] T. Sinha, M. V. Munot, and R. Sreemathy, "An efficient approach for detection of autism spectrum disorder using electroencephalography signal," *IETE J. Res.*, vol. 68, no. 2, pp. 824–832, Jun. 2019, doi: 10.1080/03772063.2019.1622462.

[12] J. J. Esqueda-Elizondo, R. Juárez-Ramírez, O. R. López-Bonilla, E. E. García-Guerrero, G. M. Galindo-Aldana, L. Jiménez-Beristáin, A. Serrano-Trujillo, E. Tlelo-Cuautle, and E. Inzunza-González, "Attention measurement of an autism spectrum disorder user using EEG signals: A case study," *Math. Comput. Appl.*, vol. 27, no. 2, p. 21, Mar. 2022, doi: 10.3390/mca27020021.

[13] N. Alotaibi and K. Maharatna, "Classification of autism spectrum disorder from EEG-based functional brain connectivity analysis," *Neural Comput.*, vol. 33, no. 7, pp. 1914–1941, Jun. 2021, doi: 10.1162/neco_a_01394.

[14] M. T. Sadiq, H. Akbari, S. Siuly, Y. Li, and P. Wen, "Alcoholic EEG signals recognition based on phase space dynamic and geometrical features," *Chaos, Solitons Fractals*, vol. 158, May 2022, Art. no. 112036, doi: 10.1016/j.chaos.2022.112036.

[15] H. Akbari, M. T. Sadiq, M. Payan, S. S. Esmaili, H. Baghri, and H. Bagheri, "Depression detection based on geometrical features extracted from SODP shape of EEG signals and binary PSO," *Traitement du Signal*, vol. 38, no. 1, pp. 13–26, Feb. 2021, doi: 10.18280/ts.380102.

[16] H. Akbari, M. T. Sadiq, N. Jafari, J. Too, N. Mikaeilvand, A. Cicone, and S. Serra-Capizzano, "Recognizing seizure using Poincaré plot of EEG signals and graphical features in DWT domain," *Bratislava Med. J.*, vol. 124, no. 1, pp. 12–24, 2022, doi: 10.4149/bll_2023_002.

[17] S. Peketi and S. B. Dhok, "Machine learning enabled P300 classifier for autism spectrum disorder using adaptive signal decomposition," *Brain Sci.*, vol. 13, no. 2, p. 315, Feb. 2023, doi: 10.3390/brainsci13020315.

[18] M. T. Sadiq, X. Yu, Z. Yuan, M. Z. Aziz, N. u. Rehman, W. Ding, and G. Xiao, "Motor imagery BCI classification based on multivariate variational mode decomposition," *IEEE Trans. Emerg. Topics Comput. Intell.*, vol. 6, no. 5, pp. 1177–1189, Oct. 2022, doi: 10.1109/TETCI.2022.3147030.

[19] A. K. Subudhi, M. Mohanty, S. K. Sahoo, S. K. Mohanty, and B. Mohanty, "Automated delimitation and classification of autistic disorder using EEG signal," *IETE J. Res.*, vol. 69, no. 2, pp. 951–959, Nov. 2020, doi: 10.1080/03772063.2020.1844076.

[20] M. Baygin, S. Dogan, T. Tuncer, P. Datta Barua, O. Faust, N. Arunkumar, E. W. Abdulhay, E. Emma Palmer, and U. Rajendra Acharya, "Automated ASD detection using hybrid deep lightweight features extracted from EEG signals," *Comput. Biol. Med.*, vol. 134, Jul. 2021, Art. no. 104548, doi: 10.1016/j.compbiomed.2021.104548.

[21] Q. M. ud Din and A. K. Jayanthy, "Automated classification of autism spectrum disorder using EEG signals and convolutional neural networks," *Biomed. Eng., Appl., Basis Commun.*, vol. 34, no. 2, Mar. 2022, Art. no. 2250020, doi: 10.4015/s101623722250020x.

[22] M. T. Sadiq, M. Z. Aziz, A. Almogren, A. Yousaf, S. Siuly, and A. U. Rehman, "Exploiting pretrained CNN models for the development of an EEG-based robust BCI framework," *Comput. Biol. Med.*, vol. 143, Apr. 2022, Art. no. 105242, doi: 10.1016/j.compbiomed.2022.105242.

[23] M. N. A. Tawhid, S. Siuly, and H. Wang, "Diagnosis of autism spectrum disorder from EEG using a time–frequency spectrogram image-based approach," *Electron. Lett.*, vol. 56, no. 25, pp. 1372–1375, Oct. 2020, doi: 10.1049/el.2020.2646.

[24] M. N. A. Tawhid, S. Siuly, H. Wang, F. Whittaker, K. Wang, and Y. Zhang, "A spectrogram image based intelligent technique for automatic detection of autism spectrum disorder from EEG," *PLoS ONE*, vol. 16, no. 6, Jun. 2021, Art. no. e0253094, doi: 10.1371/journal.pone.0253094.

[25] M. T. Sadiq, X. Yu, Z. Yuan, F. Zeming, A. U. Rehman, I. Ullah, G. Li, and G. Xiao, "Motor imagery EEG signals decoding by multivariate empirical wavelet transform-based framework for robust brain–computer interfaces," *IEEE Access*, vol. 7, pp. 171431–171451, 2019, doi: 10.1109/ACCESS.2019.2956018.

[26] M. T. Sadiq, X. Yu, Z. Yuan, M. Z. Aziz, S. Siuly, and W. Ding, "Toward the development of versatile brain–computer interfaces," *IEEE Trans. Artif. Intell.*, vol. 2, no. 4, pp. 314–328, Aug. 2021, doi: 10.1109/TAI.2021.3097307.

[27] X. Yu, M. Z. Aziz, M. T. Sadiq, Z. Fan, and G. Xiao, "A new framework for automatic detection of motor and mental imagery EEG signals for robust BCI systems," *IEEE Trans. Instrum. Meas.*, vol. 70, pp. 1–12, 2021, doi: 10.1109/TIM.2021.3069026.

[28] M. T. Sadiq, X. Yu, Z. Yuan, and M. Z. Aziz, "Motor imagery BCI classification based on novel two-dimensional modelling in empirical wavelet transform," *Electron. Lett.*, vol. 56, no. 25, pp. 1367–1369, Dec. 2020, doi: 10.1049/el.2020.2509.

[29] F. A. Alturki, M. Aljalal, A. M. Abdurraqeeb, K. Alsharabi, and A. A. Al-Shamma'a, "Common spatial pattern technique with EEG signals for diagnosis of autism and epilepsy disorders," *IEEE Access*, vol. 9, pp. 24334–24349, 2021, doi: 10.1109/ACCESS.2021.3056619.

[30] M. J. Antony, B. P. Sankaralingam, R. K. Mahendran, A. A. Gardezi, M. Shafiq, J.-G. Choi, and H. Hamam, "Classification of EEG using adaptive SVM classifier with CSP and online recursive independent component analysis," *Sensors*, vol. 22, no. 19, p. 7596, Oct. 2022, doi: 10.3390/s22197596.

[31] J. Hwang, S. Park, and J. Chi, "Improving multi-class motor imagery EEG classification using overlapping sliding window and deep learning model," *Electronics*, vol. 12, no. 5, p. 1186, Mar. 2023, doi: 10.3390/electronics12051186.

[32] M. A. A Mohamed, S. Mansour, P. Soulatiantork, K. K. Ang, P. K. Soon, and M. Arvaneh, "Improving common spatial patterns in brain-computer interface using dynamic time warping and EEG normalization," in *Proc. IEEE Int. Conf. Metrology eXtended Reality, Artif. Intell. Neural Eng. (MetroXRAINE)*, Oct. 2023, pp. 1027–1032, doi: 10.1109/metroxraine58569.2023.10405776.

[33] M. Moufassih, O. Tarahi, S. Hamou, S. Agounad, and H. I. Azami, "Boosting motor imagery brain-computer interface classification using multiband and hybrid feature extraction," *Multimedia Tools Appl.*, vol. 83, no. 16, pp. 49441–49472, Nov. 2023, doi: 10.1007/s11042-023-17118-7.

[34] P. Rithwik, V. K. Benzy, and A. P. Vinod, "High accuracy decoding of motor imagery directions from EEG-based brain computer interface using filter bank spatially regularised common spatial pattern method," *Biomed. Signal Process. Control*, vol. 72, Feb. 2022, Art. no. 103241, doi: 10.1016/j.bspc.2021.103241.

[35] Y. Shang, X. Gao, and A. An, "Multi-band spatial feature extraction and classification for motor imaging EEG signals based on OSFBCSP-GAO-SVM model," *Med. Biol. Eng. Comput.*, vol. 61, no. 6, pp. 1581–1602, Feb. 2023, doi: 10.1007/s11517-023-02793-3.

[36] F. Wang, Z. Xu, W. Zhang, S. Wu, Y. Zhang, J. Ping, and C. Wu, "Motor imagery classification using geodesic filtering common spatial pattern and filter-bank feature weighted support vector machine," *Rev. Sci. Instrum.*, vol. 91, no. 3, Mar. 2020, Art. no. 034106, doi: 10.1063/1.5142343.

[37] K. Wang, M. Xu, Y. Wang, S. Zhang, L. Chen, and D. Ming, "Enhance decoding of pre-movement EEG patterns for brain–computer interfaces," *J. Neural Eng.*, vol. 17, no. 1, Jan. 2020, Art. no. 016033, doi: 10.1088/1741-2552/ab598f.
[38] S. Z. Zahid, M. Aqil, M. Tufail, and M. S. Nazir, "Online classification of multiple motor imagery tasks using filter bank based maximum-a-posteriori common spatial pattern filters," *IRBM*, vol. 41, no. 3, pp. 141–150, Jun. 2020, doi: 10.1016/j.irbm.2019.11.002.
[39] J. Zhang, X. Wang, B. Xu, Y. Wu, X. Lou, and X. Shen, "An overview of methods of left and right foot motor imagery based on Tikhonov regularisation common spatial pattern," *Med. Biol. Eng. Comput.*, vol. 61, no. 5, pp. 1047–1056, Jan. 2023, doi: 10.1007/s11517-023-02780-8.
[40] S. Zhang, Z. Zhu, B. Zhang, B. Feng, T. Yu, Z. Li, Z. Zhang, G. Huang, and Z. Liang, "Overall optimization of CSP based on ensemble learning for motor imagery EEG decoding," *Biomed. Signal Process. Control*, vol. 77, Aug. 2022, Art. no. 103825, doi: 10.1016/j.bspc.2022.103825.
[41] I. D. Lins, L. M. M. Araújo, C. B. S. Maior, P. M. D. S. Ramos, M. J. D. C. Moura, A. J. Ferreira-Martins, R. Chaves, and A. Canabarro, "Quantum machine learning for drowsiness detection with EEG signals," *Process Saf. Environ. Protection*, vol. 186, pp. 1197–1213, Jun. 2024, doi: 10.1016/j.psep.2024.04.032.
[42] G. Aksoy, G. Cattan, S. Chakraborty, and M. Karabatak, "Quantum machine-based decision support system for the detection of schizophrenia from EEG records," *J. Med. Syst.*, vol. 48, no. 1, Mar. 2024, Art. no. 29, doi: 10.1007/s10916-024-02048-0.
[43] H. G. Enad and M. A. Mohammed, "Cloud computing-based framework for heart disease classification using quantum machine learning approach," *J. Intell. Syst.*, vol. 33, no. 1, Apr. 2024, Art. no. 20230261, doi: 10.1515/jisys-2023-0261.
[44] D. Garg, G. K. Verma, and A. K. Singh, "EEG-based emotion recognition using quantum machine learning," *Social Netw. Comput. Sci.*, vol. 4, no. 5, Jun. 2023, Art. no. 480, doi: 10.1007/s42979-023-01943-6.
[45] S. S. Kavitha and N. Kaulgud, "Quantum machine learning for support vector machine classification," *Evol. Intell.*, vol. 17, no. 2, pp. 819–828, Jul. 2022, doi: 10.1007/s12065-022-00756-5.
[46] Y. Qian, X. Wang, Y. Du, X. Wu, and D. Tao, "The dilemma of quantum neural networks," *IEEE Trans. Neural Netw. Learn. Syst.*, vol. 35, no. 4, pp. 5603–5615, Apr. 2024, doi: 10.1109/TNNLS.2022.3208313.
[47] Y. Kumar, A. Koul, P. S. Sisodia, J. Shafi, K. Verma, M. Gheisari, and M. B. Davoodi, "Heart failure detection using quantum-enhanced machine learning and traditional machine learning techniques for internet of artificially intelligent medical things," *Wireless Commun. Mobile Comput.*, vol. 2021, no. 1, pp. 1–16, Dec. 2021, doi: 10.1155/2021/1616725.
[48] H. Gupta, H. Varshney, T. K. Sharma, N. Pachauri, and O. P. Verma, "Comparative performance analysis of quantum machine learning with deep learning for diabetes prediction," *Complex Intell. Syst.*, vol. 8, no. 4, pp. 3073–3087, May 2021, doi: 10.1007/s40747-021-00398-7.

S. SARANYA received the M.E. degree in mobile and pervasive computing from Anna University, India. She is currently pursuing the Ph.D. degree with the School of Electronics Engineering, Vellore Institute of Technology, Chennai, India. Her research interests include machine learning, and biomedical signal processing.

R. MENAKA received the master's degree in applied electronics and the Ph.D. degree from Anna University, Chennai, India. She is currently a Professor with the Centre for Cyber Physical Systems, Vellore Institute of Technology, Chennai. She has published around 80 papers in peer-reviewed journals and conferences. Her areas of research interests include biomedical image and signal processing, neural networks, and fuzzy logic.